Cascaded geometric parametric process in a tapered air–silica graded-like multimode microstructure fiber

Richard Dupiol, K. Krupa, A. Tonello, Y. Arosa, T. Mansuryan, S. Fevrier, M. Fabert, D. Modotto, S. Wabnitz, G. Millot, et al.

Cascaded geometric parametric process in a tapered air–silica graded-like multimode microstructure fiber

R. Dupiol,[1,2] K. Krupa,[3] A. Tonello,[1] Y. Arosa,[4] T. Mansuryan,[1] S. Fevrier,[1] M. Fabert,[1] D. Modotto,[5] S. Wabnitz,[6] G. Millot,[2,7] and V. Couderc[1,*]

[1] Université de Limoges, XLIM, UMR CNRS 7252, 123 Avenue A. Thomas, 87060 Limoges, France
[2] Université de Bourgogne, ICB, UMR CNRS 6303, 9 Avenue A. Savary, 21078 Dijon, France
[3] Institute of Physical Chemistry, Polish Academy of Sciences, Ul. Kasprzaka 44/52, 01-224 Warsaw, Poland
[4] Departamento de Física Aplicada, Universidade de Santiago de Compostela, 15705 Santiago de Compostela, Spain
[5] Dipartimento di Ingegneria dell'Informazione, Università di Brescia, via Branze 38, 25123 Brescia, Italy
[6] Department of Information Engineering, Electronics, and Telecomm., Sapienza University of Rome, Via Eudossiana 18, 00184 Rome, Italy
[7] Institut Universitaire de France (IUF), 1 Rue Descartes, 75231 Paris, France
*vincent.couderc@xlim.fr

We experimentally study the spatial beam profile and the spectral broadening at the output of a multimode air–silica microstructure fiber taper, used along the direction of an increasing fiber diameter. By using a laser pump at 1064 nm emitting 60 ps Gaussian beam pulses, we observed a competition between Raman beam cleanup and Kerr beam self-cleaning: the multimode frequency conversion process permits to generate spectral sidebands with frequency detuning from the pump that are difficult to obtain in standard graded-index multimode fibers. The generated supercontinuum spans from 500 nm up to 2.5 µm.

https://doi.org/10.1364/OL.529507

Recent breakthroughs in the nonlinear dynamics of standard multimode fibers (MMFs) have fueled further investigations in diverse phenomena based on four-wave mixing (FWM) processes, e.g., spatial beam self-cleaning [1] or geometric parametric instability (GPI) [2]. In graded-index (GRIN) fibers, the nonlinear dynamics exploits the spatial self-imaging which is similar to the Talbot effect [3], in combination with Kerr nonlinearity, to produce an instantaneous longitudinal refractive index modulation able to phase-match spectral and spatial FWM processes, leading to supercontinuum generation or self-cleaning, respectively. The additional contribution of self-phase modulation (SPM), cross-phase modulation (XPM), modulation instability (MI), and stimulated Raman scattering (SRS) may also lead to more intricate phenomena, such as multimode solitons [4], controllable spatiotemporal nonlinear effects [5], Raman beam cleanup [6], and spatiotemporal mode-locking. [7,8].

Cascaded frequency conversion by intermodal four-wave mixing (IMFWM) may, in turn, lead to supercontinuum generation (SCG): such process has been observed by Dupiol *et al.* in a few-mode GRIN fiber [9]. Yuan *et al.* reported the cascaded frequency conversion in a multimode photonic crystal fiber (MPCF) [10,11]. Moreover, by pumping with femtosecond pulses at 800 nm, they were able to generate high power SC, with an emission of new wavelengths in the ultraviolet domain. However, frequency conversion with large spectral detuning up to 120 THz [2] has been also observed, whereas small or intermediate frequency shifts from the pump are difficult to obtain by multimode FWM.

In this work, we show how the use of MPCF with tailored refractive index profile [12] may generate multimode FWM with lower frequency detuning from the pump while maintaining a high degree of confinement within a fiber core as small as 25 µm, which is not the case in standard multimode GRIN fibers. Our microstructured MMF also leads to spatial Kerr self-cleaning and Raman beam cleanup, whose combined action initiates a cascaded FWM conversion, where the pump is depleted by SRS. Combining a MPCF with a 1064 nm laser pump permits to generate sidebands in the spectral range between 900 and 950 nm. Obtaining optical pulses in this spectral range is of particular interest for multiphoton fluorescence imaging [13]. Additionally, pulses in the 900–950 nm spectral range can be used to pump semiconductor quantum dots, a promising technology for single-photon sources in the 920–980 nm window with count rates up to 10 MHz, efficient indistinguishability (above 95%), and low multiphoton contributions [14].

Fibers tapered in the acceleration and deceleration regimes of the nonlinearity, i.e. from large to small core diameters or vice versa, have already been studied: Eftekhar *et al.* [15] demonstrated spatiotemporal acceleration in the region of anomalous dispersion, leading to blueshifted multimode solitons and dispersive wave combs; Niang *et al.* [16,17] also obtained self-cleaning and SCG both in deceleration and acceleration regimes in an Ytterbium-doped tapered MMF.

In our work, we used a MPCF with a similar transverse structure as the one described in [12]. The fiber preform is composed of rods of silica glass and concentric rings of air holes, whose diameters increase when moving outward from the center, in order to reduce the local average refractive index as the volume of air grows larger. Such arrangement, which is suitable for

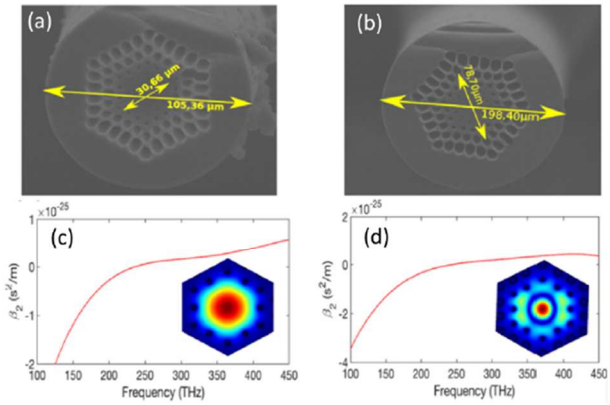

Fig. 1. (a) and (b) SEM picture of (a) the smallest and (b) the largest diameter of the tapered microstructured MMF; numerically calculated intensity of (c) mode 1 and (d) mode 2 at 1064 nm and their dispersion curves.

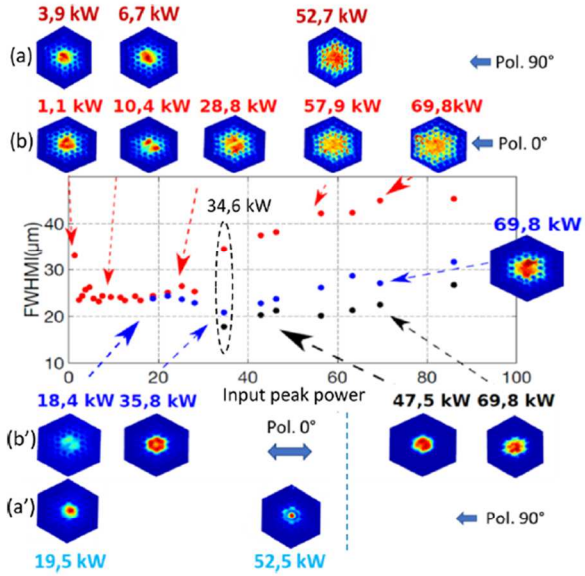

Fig. 2. Input peak power evolution of the beam diameter for the pump [red dots—top lines, for (a) 90° and (b) 0° of input polarizations (Pol)], the first Raman Stokes at 1117 nm [blue dots—bottom lines (left) for (a') 90° and (b') 0° of input polarizations (Pol)] and the second Raman Stokes at 1175 nm [black dots—bottom lines (right) for 0° only of input polarizations (Pol)]; insets: corresponding output beam patterns for different input peak powers for a 20 m long fiber.

the stack and draw technique, is reminiscent of the refractive index profile of GRIN fibers or tapers that are usually obtained by preforms prepared by chemical vapor deposition. While the first parametric sidebands exhibit a lower frequency detuning from the pump than that in Ref. [2], our microstructure fiber still allows for efficient generation of multiple sidebands and SCG. The competition with the Raman effect limits the efficiency of parametric process to a fixed fiber length: upon pump depletion, a sideband, generally at shorter wavelength, can become a secondary pump. The particular air-hole structure permits to generate the first Stokes and anti-Stokes waves at a frequency detuning lower than the GPI in commercial GRIN fibers, with typical core diameters of 10–100 µm.

We considered a 20 m long MMF taper, with a diameter continuously varying between the two output facets from a maximum of 40.61 µm to a minimum of 25.16 µm. Panels (a) and (b) of Fig. 1 show the scanning electron microscope (SEM) images of the smallest and largest fiber diameter, respectively. The effective indices and mode profiles have been calculated by using a mode solver (COMSOL Multiphysics). Panels (c) and (d) of Fig. 1 show the numerically calculated transverse profiles and the corresponding dispersion curves of the first two guided modes. The mode solver predicts the existence at 1064 nm of 40 (65) guided modes for the smallest (largest) core diameter. The size of the fundamental mode [see Fig. 1(c)] at a full width at half-maximum in intensity, FWHMI, is of 16.77 µm (smallest core diameter) and of 27.07 µm (largest core diameter): at both sides of the taper the modal area covers approximately two thirds of the total core surface.

We used the experimental setup already described in Ref. [12]. A linearly polarized picosecond laser at 1064 nm (60 ps, 20 kHz) is driven by an optical power controller. A positive lens imaged the laser beam on the entrance face of the fiber with a beam diameter of 30 µm. In particular, by using a 40 mm converging lens, we obtained a coupling efficiency close to 40%. We measured the spectrum with two optical spectral analyzers: Ando (AQ6315E) and Yokogawa (AQ6376) covering the range 350–3.2 µm, with 0.05 nm resolution.

In a first series of experiments, we studied the power dependence of the output beam shape at the pump wavelength of 1064 nm, as well as at the first (1117 nm) and at the second (1175 nm) Raman Stokes sidebands. These three spectral components have been selected with three different 10 nm wide bandpass filters, placed in between the fiber output and the camera. The input peak power was varied by about two orders of magnitude, from 1.1 kW up to about 86 kW. Figure 2 summarizes the evolution of the beam diameters and transverse beam shapes upon power, measured at the output of the 20 m long fiber taper. At relatively low powers (quasi-linear propagation regime) the output profile at 1064 nm exhibits a sort of triangular shape, with a FWHMI beam diameter of 33 µm (red dots in Fig. 2).

When increasing the input pump power above 6.7 kW (see Fig. 2), the nonlinear Kerr self-cleaning effect leads to the reduction of the output beam diameter down to 23.2 µm (in short, light is entirely confined by the innermost silica core of the fiber), with a dual-lobe beam shape similar to an LP_{11} mode. Such beam shape persists, albeit with a larger area, up to 30 kW of input power. We also noted that, by changing the input polarization state, the output beam shape may evolve toward a state with a maximum beam intensity in the center, i.e., close to the fundamental mode (see insets of Fig. 2). Above 30 kW, the diameter of the output pump beam expands until it doubles its diameter at 57.9 kW. As already discussed in [12], SRS introduces a strong energy depletion in the central part of the beam while leaving nearly unchanged its outer part [which mostly contains high-order modes (HOMs)]. From a different perspective, SRS can be interpreted as a nonlinear eclipser: by depleting the innermost part of the beam with the largest power density, it reveals the natural tendency of nonlinear multimode beam interactions to spread the power toward the HOM. Figure 2 also demonstrates that the diameter of the first Stokes beam (blue dots) shrinks down to about 20.8 µm as the pump power grows up to 34.6 kW. Such a value shows that the SRS frequency conversion is indeed

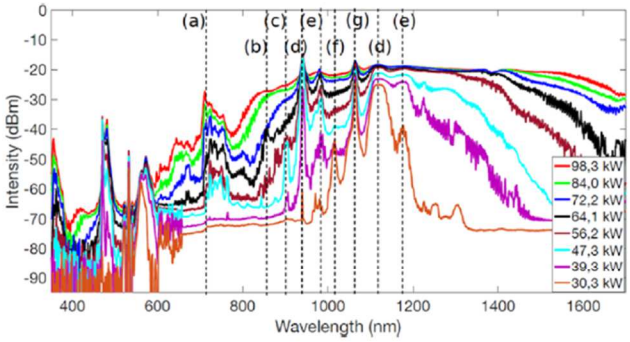

Fig. 3. Output spectrum for different input peak powers. Dashed lines correspond to the following wavelengths [detuning from the pump: (a) 710.5 nm (140.3 THz), (b) 842.6 nm (74.1 THz), (c) 903.5 nm (50.1 THz), (d) 942.6 nm (36.3 THz), (e) 971 nm (27 THz), (f) 1016 nm (13.3 THz), (g) 1064 nm, (h) 1118 nm (13.6 THz), and (i) 1175 nm (26.6 THz)].

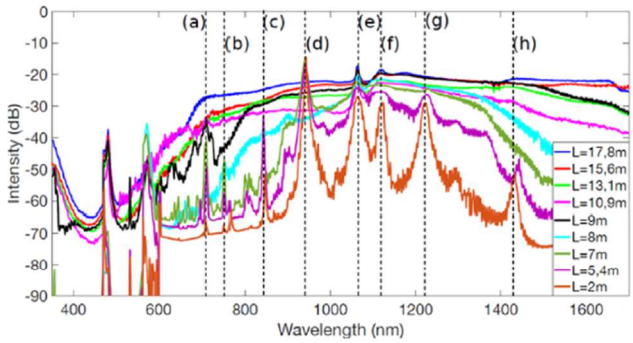

Fig. 4. Output spectrum for different fiber lengths (input peak power: 106.3 kW). Dashed lines correspond to the following wavelengths [detuning from the pump: (a) 710.5 nm (140.2 THz), (b) 753.6 nm (116.1 THz), (c) 842.6 nm (74.0 THz), (d) 942.6 nm (36.3 THz), (e) 1064 nm, (f) 1118 nm (13.2 THz), (g) 1222 nm (36.4 THz), and (h) 1442 nm (73.9 THz)].

accompanied by Stokes beam cleanup, which is typically not observed in step-index fibers [6]; however, it is present in our case because of the radially evolving microstructure. For input pump powers beyond 34.6 kW, the diameter of the first Stokes sideband grows larger. Note that this spatial beam expansion is accompanied by the generation of a second order Stokes wave: the corresponding depletion of the first order Stokes beam leads to an increase of its diameter.

Figure 3 illustrates the evolution of the output spectrum as function of input peak power. At the lowest power level of 30.3 kW, we notice the presence of two Raman Stokes bands (see also the experimental point at 34.6 kW in Fig. 2). Two anti-Stokes Raman bands at 1016 nm (13.3 THz) and 971 nm (27 THz) are also observed. At 39.3 kW, a sideband at 942.6 nm appears and reaches almost the same intensity as the pump at 1064 nm. Such a high conversion efficiency can produce a beam that is sufficiently strong for direct use for several applications. For longer propagation distances, further cascaded generation of other wavelengths is also possible. Indeed, starting from a pump power of 47.3 kW, the sideband level at 942.6 nm saturates, leading to the generation of a new sideband at 710.5 nm, whose intensity increases when the input power grows larger. Such a dynamic is reminiscent of a cascaded IMFWM process.

We numerically calculated the phase mismatch for several different combinations of FWM by assuming that the 942.6 nm sideband acts as a secondary pump. We started by a modal configuration of a degenerate FWM, with the two pump photons carried by mode 1. When considering the different combinations, we found a good agreement with the experimental data when anti-Stokes and Stokes waves are carried by mode 2 and mode 1, respectively. The corresponding phase-matching calculation gives a frequency detuning of 101.3 THz, which yields anti-Stokes and Stokes waves at 714.8 and 1383.4 nm, respectively. In a third series of experiments, as illustrated in Fig. 4, we fixed the input peak power to 106.3 kW, and we measured the evolution of the spectrum as a function of the propagation distance by using a cut-back method. As can be seen, a first nonlinear frequency conversion takes place after 2 m owing to a modal FWM process [12], generating Stokes and anti-Stokes waves at 1222 and 942.6 nm, respectively.

These wavelengths agree well with predictions obtained from the FWM phase-matching conditions, when considering the previously applied combination of modes 1 and 2 for the pump, Stokes, and anti-Stokes waves, but with a pump at 1064 nm. Indeed, we obtained a 38.6 THz frequency detuning from the pump, leading to the predicted 935.8 and 1232.9 nm wavelengths for the anti-Stokes and Stokes sidebands, respectively. For our calculations, we assumed the largest core diameter as the light propagation was in that direction.

At a 2-m distance in the fiber, one may also notice the existence of other sidebands, such as the first Raman Stokes wave; particularly interesting are the sidebands at 1442 and 842.6 nm. Analytical calculations can explain that those peaks fulfill the FWM phase-matching when the two pump photons are in two different modes, i.e., in mode 1 and mode 2. We calculated a frequency detuning with respect to the pump of 77.2 THz, which corresponds to anti-Stokes and Stokes lines at 835.2 and 1465.5 nm, respectively.

For fiber lengths beyond 2 m, as illustrated in Fig. 4, we observed a strong SRS frequency conversion into the first Stokes wave at 1118 nm, which drastically depletes the pump beam, thus reducing the efficiency of parametric processes. For longer fiber lengths, we observed a progressive extension of the near-infrared spectrum (see Fig. 4). For a fiber length close to 18 m, a continuum ranging from 700 nm up to 1700 nm was generated. On the visible side of the spectrum, the most powerful frequency components were located at 710.5 nm (i.e., 140.2 THz from the pump) and 753.6 nm (i.e. 116.1 THz from the pump), which are mainly carried by mode 2 (see Fig. 5). In Fig. 5, we present the output beam shapes measured at different wavelengths for the SC generated by a 20 m long tapered microstructure MMF at 98.3 kW of input peak power. Let us remind that SC is generated by a complex interplay of a multitude of different nonlinear effects. In the spectrum displayed in Fig. 5, we still observe the trace of the powerful first anti-Stokes parametric sideband at 942.6 nm. We may also observe a well-identified sideband at 710.5 nm, which is also generated by an IMFWM process in agreement with the results of Fig. 3. The spatial patterns in the inset of Fig. 5 were measured with a series of 10 nm bandpass filters in combination with the CCD and CMOS cameras to cover the spectral range 700–1600 nm.

We may observe that at certain wavelengths, especially in the infrared domain, the spatial shape tends toward the fundamental mode 1, [see Fig. 1(c)]. Whereas, mode 2 intensifies in the visible domain [Fig. 1(d)]. This observation confirms the modal

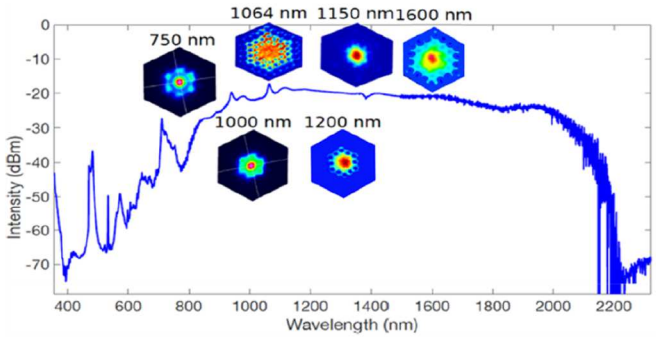

Fig. 5. Spatial evolution of the beam profile for different wavelengths along the seeded SC at 98.3 kW (fiber length of 20 m).

composition of our phase-matching calculation for IMFWM, as illustrated in Figs. 3 and 4.

In conclusion, we studied nonlinear beam shaping, frequency conversion, and supercontinuum generation in a tapered multimode microstructure fiber with a graded-like profile, used in the nonlinearity deceleration regime. We first observed the coexistence of Kerr self-cleaning and Raman beam cleanup, which concentrate both the input pulse energy and the frequency-converted wavelengths on low-order modes. We observed an efficient frequency conversion across the visible and the near-infrared windows owing to the cascaded IMFWM driven by Raman pump depletion. We have shown that an initial FWM, involving the pump at 1064 nm can, at high powers, be superseded by a new FWM process pumped by the first anti-Stokes sideband at 942 nm in the strong conversion regime. The phase-matching calculations agree well with experiments and directly depend on the local core diameter varying from 25 to 40 µm. For application perspectives, our results open a new route for efficient frequency conversion in tapered microstructure multimode fibers with controllable frequency shift.

Funding. Narodowe Centrum Nauki (OPUS 2023/49/B/ST7/01482); Horizon 2020 Framework Programme [Horizon 2020 ERC AdG (No. 740355)]; Consellería de Cultura, Educación e Ordenación Universitaria, Xunta de Galicia (ED481B-2021-027); Conseil Régional Aquitaine (Naquidis center); Agence Nationale de la Recherche (3Dmoc project ANR-23-CE08-0021-02, ANR-10-LABX-0074, Equipex ADD4P ANR-21-ESRE-0007).

Disclosures. The authors declare no conflicts of interest.

Data availability. Data underlying the results presented in this paper may be obtained from the authors upon reasonable request.

REFERENCES

1. K. Krupa, A. Tonello, B. M. Shalaby, *et al.*, Nat. Photonics **11**, 237 (2017).
2. K. Krupa, A. Tonello, A. Barthélémy, *et al.*, Phys. Rev. Lett. **116**, 183901 (2016).
3. H. Talbot, The London, Edinburgh, and Dublin Philosophical Magazine and Journal of Science **9**, 401 (1836).
4. Z. Zhu, L. G. Wright, D. N. Christodoulides, *et al.*, Opt. Lett. **41**, 4819 (2016).
5. L. G. Wright, D. N. Christodoulides, and F. W. Wise, Nat. Photonics **9**, 306 (2015).
6. N. B. Terry, T. G. Alley, and T. H. Russell, Opt. Express **15**, 17509 (2007).
7. L. G. Wright, D. N. Christodoulides, and F. W. Wise, Science **358**, 94 (2017).
8. R. Guenard, K. Krupa, R. Dupiol, *et al.*, Opt. Express **25**, 22219 (2017).
9. R. Dupiol, A. Bendahmane, K. Krupa, *et al.*, Opt. Lett. **42**, 3419 (2017).
10. J. Yuan, Z. Kang, F. Li, *et al.*, Opt. Lett. **40**, 1338 (2015).
11. J. Yuan, Z. Kang, F. Li, *et al.*, Opt. Lett. **42**, 3537 (2017).
12. R. Dupiol, K. Krupa, and A. Tonello, Opt. Lett. **43**, 587 (2018).
13. J. Choi, M.-S. Choi, J. Jeon, *et al.*, Biomed. Opt. Express **14**, 1647 (2023).
14. G. S. Solomon, E. B. Flagg, S. V. Polyakov, *et al.*, J. Opt. Soc. Am. B **29**, 319 (2012).
15. M. A. Eftekhar, Z. Sanjabi-Eznaveh, H. E. Lopez-Aviles, *et al.*, Nat. Commun. **10**, 1638 (2019).
16. A. Niang, D. Modotto, A. Tonello, *et al.*, IEEE Photonics J. **12**, 1 (2020).
17. A. Niang, T. Mansuryan, K. Krupa, *et al.*, Opt. Express **27**, 24018 (2019).